Journal of Southeast University (English Edition) Vol. 22, No. 2, pp. 273 - 280 June 2006 ISSN 1003—7985

Complementary system-theoretic modelling approach for enhancing hydrological forecasting

Martins Y. Otache Li Zhijia

(State Key Laboratory of Hydrology-Water Resources and Hydraulic Engineering, Hohai University, Nanjing 210098, China)

Abstract: Hydrologic models generally represent the most dominant processes since they are mere simplifications of physical reality and thus are subject to many significant uncertainties. As such, a coupling strategy is proposed. To this end, the coupling of the artificial neural network (ANN) with the Xin'anjiang conceptual model with a view to enhance the quality of its flow forecast is presented. The approach uses the latest observations and residuals in runoff/discharge forecasts from the Xin'anjiang model. The two complementary models (Xin'anjiang & ANN) are used in such a way that residuals of the Xin'anjiang model are forecasted by a neural network model so that flow forecasts can be improved as new observations come in. For the complementary neural network, the input data were presented in a patterned format to conform to the calibration regime of the Xin'anjiang conceptual model, using differing variants of the neural network scheme. The results show that there is a substantial improvement in the accuracy of the forecasts when the complementary model was operated on top of the Xin'anjiang conceptual model as compared with the results of the Xin'anjiang model alone.

Key words: hydrological forecasting; complementary model; residual; Xin'anjiang conceptual model; artificial neural network

In view of the fact that conceptual models are simplifications of physical systems, they are obviously susceptible to error. In order to extenuate these conceptual problems and enhance the chances of better forecasts, the idea of complementary modelling comes in handy and seemingly becomes an attractive alternative approach. Thus, how efficient in terms of time utilization and ease of computation vis-à-vis the overall desire for a better forecast in view of the nature of the issues that constitute the underlying essence of forecasting becomes the subject matter of this research.

The very basis of the above reasoning is derived by the fact that system-theoretic or data-driven models are neither based on an explicit representation of discrete physical processes nor a pre-conceived conceptualization of the behaviour of the system. But rather, they are based on the relationship between selected input and output sets of data. In consequence, they are limited to learning from the data provided. Inferentially, it is clear that the two models are characterized by inherent limitations.

Considering these deficiencies or shortcomings, it is paramount to note that these models should not be operated on a stand-alone basis if the operational environment allows. To achieve this end, the artificial neural network (ANN), a system-theoretic model was used to update the Xin'anjiang model forecast after being calibrated by a faster optimization method in a coupling strategy; in this case, the Shuffle complex evolutionary (SCE) algorithm is used. The underlying reason for this approach derives from the single fact that "once a complementary model is established for a conceptual model, the complementary model is independent of the main model; the complementary model can incorporate input data that the conceptual model is not structured to take"[1].

1 Research Objectives

The central objectives of this study are as follows:

- To establish the effectiveness of the Xin'anjiang model calibration using an automatic optimization method.
- Enhancement of the quality of model runoff forecasts via coupling or complementary modelling.

2 Description of Watersheds

For this study, the Misai catchment and the Lushi basin, a sub-basin of the Guxian Reservoir were used. The Misai catchment (in Zhejiang province, China) has a total of six precipitation measuring stations iden-

Received 2005-09-15.

Biographies: Martins Y. Otache (1968—), male, graduate, Nigerian, martinso3@yahoo.com; Li Zhijia (corresponding author), male, doctor, professor, lizhija@vip.sina.com.

tified according as Qixi, Majin, Yanxi, Daxibian, Huanglinkang, and Misai, respectively (see Tab. 1).

Tab. 1 Sub-basin characteristics

Station ID	Name of the sub-catchment	Area/km^2	Area factor
1	Qixi	207. 22	0. 260
2	Majin	162. 59	0. 204
3	Yanxi	130. 71	0. 164
4	Daxibian	131. 51	0. 165
5	Huanglinkang	89. 26	0. 112
6	Misai	75. 71	0. 095

As in the preceding section, the Lushi basin is one of the two basins of the Guxian Reservoir; the second being the Linkou. The Guxian Reservoir is located in Luoning county, Henan province, China. In all, the reservoir comprised of the two basins has a network of a total of fifteen gauging stations. It is paramount to state here that according to the natural boundary condition and flow stages in this basin area, the intervening area or sections between Lushi and Linkou is divided into six sub-basins (see Tab. 2).

Tab. 2 Lushi sub-basin characteristics

Station ID	Gauging point number	Sub reach	Area/km^2	Area factor
1	8	7	257. 64	0. 120
2	9	8	364. 99	0. 170
3	10	6	536. 75	0. 250
4	11	6	279. 11	0. 130
5	12	2	343. 52	0. 160
6	13	2	364. 99	0. 170

3 The Xin'anjiang Conceptual Model

The Xin'anjiang model was developed in 1973 by the East China College of Hydraulic Engineering (now Hohai University), with the underlying aim to forecast flows to the Xin'anjiang Reservoir[2]. The Xin'anjiang model has a hierarchical structure with two distinct conceptual storages (tension water and free water) to account for soil moisture process regime in conjugal relationship with precipitation, and the consequent runoff generation and separation constituents.

4 Study Protocol

4.1 Optimization

In realization of the stated objectives of this study, for the first phase, precursory to the development of the ANN complementary model, the applicability and validity of the automatically calibrated parameter set were investigated using the SCE optimization algorithm in flood event applications.

To this end, all together, 16 flood events (3-hourly data) selected from the Misai catchment's historical data were used. The first ten flood events were used for calibration while the remaining six were used for validating the model. For the Lushi basin, a total of 14 flood events (hourly data) were selected from 29 flood events. As in the case of the Misai, the first ten flood events were similarly used for calibration while the remaining four were used for verification.

For the calibration process proper, all the parameters, except B and EX, were calibrated simultaneously using the SCE algorithm; parameters B and EX were fixed in accordance with the findings of Ref. [3]. The initial state of the catchment (Misai) for each flood event was obtained from the daily model application results[3]. In the calibration, for Misai and Lushi basins respectively, the number of complexes of the SCE algorithm was set to 42 and 40 while other algorithmic parameters were set to their default values[4]. For the Lushi basin, in the application, the inflow from the Linkou basin was routed down along the intervening flow path using the Muskingum flow routing method so as to obtain the discharge at the Lushi end.

The entire calibration process was carried out specifically under the following conditions: The tolerance is 10^{-5}; the iteration is 2×10^5; the random seed number is -87; the number of optimized parameters is 13; the number of evolution steps is 8. Considering the fact that objective functions play crucial roles in model calibration, a balanced aggregate objective function was used. To do this, four other objective functions depicting emphasis on specific aspects of the calibration were coalesced into one, herein the balanced aggregate objective function.

4.2 Development of the ANN system

4.2.1 Data base selection

The selection of the data base to train a neural network is of paramount importance; thus in this regard, for the ANN model used, the available data record was used in two and one variants for the Misai and Lushi basins, respectively. In the first and second variants (Misai), i. e., ANN model Ⅰ and ANN model Ⅱ, the whole data was split into two, corresponding to the calibration and verification modes as applied in the Xin'anjiang conceptual model. For ANN model Ⅰ, the training data consisted of 459 examples while the verification was made up of 277 exemplars. But in the second variant, ANN model Ⅱ, new input data was selected from the range of the entire data set comprising the calibration and verification data record as used in the first variant. In other words, a composite data set was

composed. It consisted of 577 examples for training while the training examples in the first variant (459 examples) were then used to validate the neural network. In the case of the Lushi basin, the whole data record was used as a single variant. The first half (1 352 examples) was for training while the second (650 examples) was for verification.

To ensure that an influential range of data input was used, the relationship between the residuals of the conceptual model and selected time series such as rainfall, discharge/runoff observations and previous model residuals was analyzed using the Pearson moment correlation. The main rationale here is the assumption that the residual time series is the best reflection of the gap between the model and the physical process it represents[1]. This was done by considering data sets that are seemed adequate and do have some level of meaningful influence on the target for the network. This assertion is glaringly evident as in the correlation matrices for both the Misai and Lushi catchments(see Tabs. 3 and 4).

Tab. 3 Correlation matrix for the Misai catchment's training data

Variables	P_t	P_{t-1}	P_{t-2}	Q_{t-1}	E_t	E_{t-1}	E_{t-2}
P_t	1	0.602	0.429	0.011	0.057	0.035	-0.029
P_{t-1}		1	0.573	0.063	0.062	0.064	0.040
P_{t-2}			1	0.113	0.071	0.065	0.067
Q_{t-1}				1	-0.005	0.210	0.177
E_t					1	0.546	0.333
E_{t-1}						1	0.546
E_{t-2}							1

Note: Matrix vectors are Pearson correlation coefficients.

Tab. 4 Correlation matrix for the Lushi catchment's training data

Variables	P_{t-1}	P_{t-2}	Q_{t-1}	Q_{t-2}	E_{t-1}	E_{t-2}	Q_t	E_t
P_{t-1}	1.000	0.862	0.113	0.095	-0.067	-0.047	0.134	-0.085
P_{t-2}		1.000	0.133	0.113	-0.085	-0.067	0.155	-0.110
Q_{t-1}			1.000	0.992	0.415	0.392	0.992	0.409
Q_{t-2}				1.000	0.409	0.415	0.975	0.390
E_{t-1}					1.000	0.935	0.392	0.935
E_{t-2}						1.000	0.357	0.813
Q_t							1.000	0.415
E_t								1.000

Note: Matrix vectors are Pearson correlation coefficients.

4.2.2 Network topology/training

The architectures of ANN models are motivated by models of biological neural networks which can recognize patterns and learn from their interactions with the environment. For this particular study therefore, a 3-layer feed-forward back-propagation neural network with bias connections has been used for the Misai and Lushi catchments, respectively. The feed-forward ANN is used herein due to its general applicability to a variety of different problems[5].

In view of the fact that the number of nodes in the input and output layers are dictated by the dimension of input and output vectors presented to the network for training, or rather the external specifications of the problem, the number of input nodes is six corresponding to the input variables and output node, one as for the Misai catchment. But for the Lushi catchment, a multi-objective output approach is adopted; here, the number of output nodes is equal to two, being the desired output variables.

After a series of trials, the best network structure deemed appropriate for the Misai catchment is given in Fig. 1. The input layer is made up of six nodes (processing elements), while the hidden layer consists of 11 nodes (processing elements) and lastly, one node in the output layer. Similarly, for the Lushi catchment, the same network structure is maintained except for the increase in the number of nodes in the hidden layer and output layer. Thus eventually, a three-layer network consisting of six input nodes, 15 nodes in the hidden layer and two nodes in the output layer was considered best suitable (see Fig. 2).

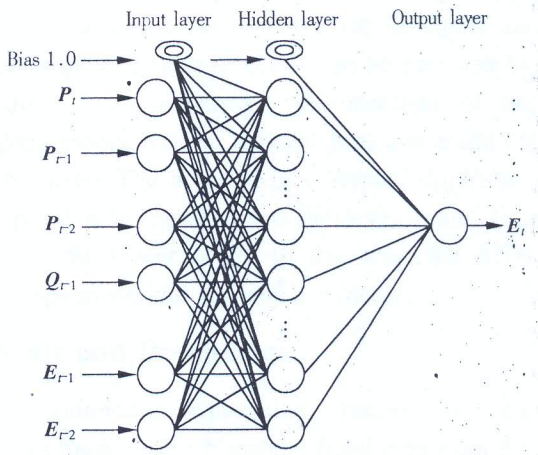

Fig. 1 ANN structure for the Misai catchment

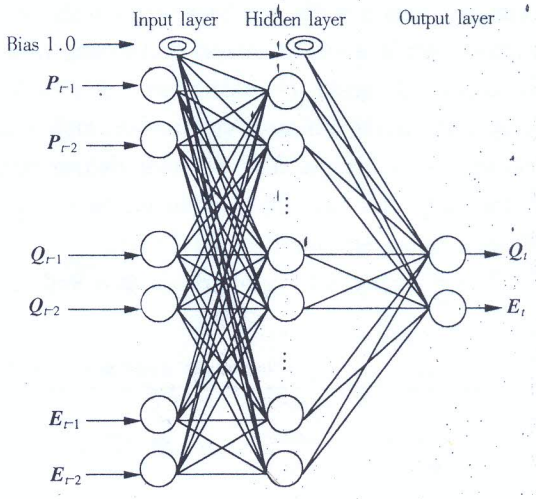

Fig. 2 ANN structure for the Lushi catchment

In line with the training process, biases and weights or connection strengths between processing units were modified through the training process and the final values represent the trained ANN. Therefore, these weights and biases were initialized. Essentially, since the transformation of the inputs to outputs was largely dependent on the transfer function; the tan sigmoid and linear (Purelin in the output nodes) transfer functions were used. The use of the tan sigmoid was to enable non-linearity of the network; however, not for the output nodes since it forces an output to be scaled by a known maximum. The practice adopted for calibration and verification is to divide the available data into two independent sets, i. e., split sampling. The first data set was used for calibration and the second for validation or verification in line with calibration and verification data sets, respectively, as used in the Xin'anjiang model forecast.

The success of the calibration procedure depends largely on the power of the optimization method used to search for the best parameter estimates; this is in line with the findings of Ref. [5]. Though Matlab routines were used for this part of the study, the Levenberg-Marquardt algorithm which is the default training function was skipped for the Bayesian regularization training algorithm because of the computational overhead of the former.

The accuracy of the results obtained from the network can be assessed by comparing its responses with the validation set by using the following performance criteria, namely, the root mean square error $\varepsilon_{\mathrm{RMSE}}$, the coefficient of efficiency R^2, and the Pearson moment correlation coefficient R.

Computationally, the root mean square error is evaluated accordingly as

$$\varepsilon_{\mathrm{RMSE}} = \left[\frac{1}{Q}\left(\sum_{q=1}^{Q}(t_q - a_q)^{\mathrm{T}}(t_q - a_q)\right)\right]^{\frac{1}{2}}$$

where t_q and a_q represent target and network prediction, respectively.

On the other hand, the overall performance of each network (i. e., both Misai and Lushi catchments) trained was judged with respect to the validation data on the basis of the coefficient of efficiency R^2 calculated as

$$R^2 = 1 - \frac{\sum_{p}(y_p - d_p)^2}{\sum_{p}(d_p - \bar{d})^2}$$

where y_p and d_p are the network predictions and target values for each pattern p, respectively; $\bar{d}$ is the mean target output.

4.2.3 Discharge updating as applied on the Xin'anjiang model

Here, the Xin'anjiang model is integrated with the ANN model operating as a post-processing module that allows for the forecast of the Xin'anjiang model forecast residual and exploits the measures of actual discharge up to the current forecast instant. The two complementary models are used in such a way that residuals of the conceptual model are forecasted by a neural network model so that runoff/discharge forecasts can be improved as new observations come in. In doing this, the residuals between simulated and observed flows of the Xin'anjiang model are targeted instead of the observed flows. Once the residuals are predicted, improved flow forecasts can be obtained by taking the difference between the forecasts of the Xin'anjiang model and the residual forecasts made by the ANN model. The adjusted or corrected discharges are compared with the observed flows Q_{obs}, and D_{obs} to establish the extent of fit. In this way, the ANN model complements the Xin'anjiang model.

5 Results and Discussion

The automatic calibration results of the Xin'anjiang model using historical flood data from the Misai and Lushi catchments as presented here precursory to the development of the ANN complementary model show contrasting twists. Analysis of the calibration results (i. e., optimization) using the 3-hourly and hourly data respectively from the Misai and Lushi catchments reveals that the SCE algorithm is capable of finding a conceptually realistic and valid parameter set (see Tabs. 5 and 6) while fixing the parameters B and EX in line with the findings of Hapuarachchi[3].

Tab. 5 Overall model performance of the flood events for the Misai catchment

Description	Calibration			Verification		
	Observed	Simulated	Corrected	Observed	Simulated	Corrected
Mean annual flow depth/(mm·d^{-1})	131. 37	122. 31	131. 37	92. 46	83. 65	92. 40
Standard deviation/(mm·d^{-1})	213. 51	208. 87	213. 51	172. 55	144. 39	171. 88
Pearson correlation		0. 970	0. 998		0. 978	0. 989

Tab. 6 Overall model performance of the flood events for the Lushi catchment

Description	Calibration				Verification			
	Q_{obs}	Q_{cal}	ANN_Q_{cal}	Q_{corr}	Q_{obs}	Q_{cal}	ANN_Q_{cal}	Q_{corr}
Mean annual flow rate/ ($m^3 \cdot s^{-1} \cdot d^{-1}$)	257.11	249.81	256.15	257.15	102.74	93.94	65.05	99.83
Standard deviation/ ($m^3 \cdot s^{-1} \cdot d^{-1}$)	329.37	304.26	326.04	329.63	137.24	108.15	200.40	135.96
Pearson correlation		0.968	0.997	0.998		0.942	0.812	0.993

The overall performance of the model (see Tabs. 5 and 6) in these two cases is excellent; especially, the attainment of high overall efficiency R^2 in the two catchments. The peak flow error (PFE) and lead lag time error (LLE) (see Tabs. 7 to 9) values of all flood events in the calibration and validation stages are acceptable, though the PFE values of the flood events 10 and 15 (see Tabs. 7 and 8) in the calibration and verification for the Misai catchment alike are quite high. This might be attributable to data errors. But for most of the events, i. e. in the two stages, the LLE value is zero indicating the coincidence of the observed and simulated peakflows (occur at the same time). The situation in this regard for Lushi is somewhat different as shown in Tabs. 9 and 10.

Tab. 7 Calibration results of the Misai catchment

Event	Date	p/mm	E/mm	D_{obs}/mm	D_{cal}/mm	ε_{RMSE}	R^2	PFE	LLE
1	19820402T11 to 19820409T05	73.0	16.3	65.0	47.0	39.47	0.70	4.06	0
2	19820717T11 to 19820724T05	86.8	27.6	37.9	41.4	26.13	0.84	10.76	-1
3	19830529T08 to 19830601T23	228.5	6.8	170.7	171.5	99.74	0.96	6.52	1
4	19830614T08 to 19830619T17	99.8	15.6	78.1	68.6	48.24	0.94	7.65	0
5	19831006T08 to 19831010T17	68.8	6.8	71.2	49.5	73.43	0.66	6.27	0
6	19840402T17 to 19840407T23	142.0	6.4	131.6	105.2	71.53	0.86	2.71	0
7	19840607T08 to 19840612T17	76.6	13.0	43.5	38.5	20.40	0.90	3.72	0
8	19850505T08 to 19850509T08	93.2	11.6	51.6	58.6	33.53	0.95	6.42	0
9	19850703T08 to 19850709T17	83.8	24.4	64.0	61.2	34.22	0.87	4.19	-2
10	19860519T05 to 19860527T17	166.4	43.0	104.3	120.1	57.57	0.94	10.05	-1

Tab. 8 Verification results of the Misai catchment

Event	Date	p/mm	E/mm	D_{obs}/mm	D_{cal}/mm	ε_{RMSE}	R^2	PFE	LLE
11	19860704T08 to 19860712T08	82.8	26.8	49.7	45.9	20.79	0.86	5.53	0
12	19870425T08 to 19870430T08	69.5	19.1	40.8	44.1	27.34	0.84	4.59	-1
13	19870526T05 to 19870530T17	62.7	19.0	38.7	29.6	24.59	0.75	3.91	0
14	19870531T05 to 19870605T17	65.8	17.8	40.7	40.8	9.38	0.97	1.64	0
15	19870909T05 to 19870914T17	65.2	8.9	24.4	18.9	13.76	0.75	16.22	1
16	19880621T08 to 19880626T23	145.6	15.1	152.4	136.9	100.39	0.93	6.55	0

Tab. 9 Verification results of the Lushi catchment

Event	Date	p/mm	E/mm	Q_{obs}/($m^3 \cdot s^{-1}$)	Q_{cal}/($m^3 \cdot s^{-1}$)	ε_{RMSE}	R^2	PFE	LLE
11	19910914T08 to 19910919T08	82.8	26.8	49.7	14.3	32.60	0.81	3.01	0
12	19920811T08 to 19920818T08	69.5	19.1	40.8	29.9	36.02	0.92	2.16	-2
13	19930720T08 to 19930727T08	62.7	19.0	38.7	15.4	23.67	0.85	3.56	0
14	19960916T08 to 19960924T08	70.6	22.4	57.3	42.7	81.22	0.80	2.03	6

Tab. 10 Calibration results of the Lushi catchment

Event	Date	p/mm	E/mm	Q_{obs}/($m^3 \cdot s^{-1}$)	Q_{cal}/($m^3 \cdot s^{-1}$)	ε_{RMSE}	R^2	PFE	LLE
1	19810904T08 to 19810914T20	74.7	16.6	125.5	128.5	33.06	0.99	0.33	-1
2	19820730T15 to 19820804T06	129.3	33.1	93.2	99.1	180.78	0.87	2.48	5
3	19840920T08 to 19840925T06	115.7	7.1	125.7	109.2	159.69	0.89	2.85	-2
4	19870604T08 to 19870606T24	71.3	7.3	29.1	27.8	105.79	0.84	4.59	4
5	19880809T08 to 19880812T15	36.4	10.1	24.8	23.9	41.07	0.88	1.92	1
6	19880817T08 to 19880821T08	53.5	10.2	67.6	68.0	84.42	0.91	1.54	-2
7	19890709T08 to 19890715T08	107.6	15.6	57.3	53.7	84.64	0.92	3.03	3
8	19890827T08 to 19890901T08	2.0	1.9	18.3	17.3	22.36	0.87	1.81	0
9	19900429T08 to 19900506T08	8.9	8.6	24.1	19.8	22.80	0.86	2.69	-1
10	19900629T08 to 19900707T08	24.2	30.1	17.6	17.1	17.82	0.87	4.31	-2

As shown in Fig. 3, the model shows a reasonable reproduction of the observed discharge for most of the flood events. However, there are observable discrepancies in some portions of the hydrograph for some of the flood events. These discrepancies are attributable to prediction errors. For the two case studies, considering the whole time series, i. e., 16 flood events for Misai and 14 for the Lushi basin, the prediction error varies between −306.57 and +300.76 and the ε_{RMSE} being 43.57 with a corresponding efficiency coefficient of 0.865 while for Lushi, the prediction error for the whole time series in continuous simulation varies between −507.85 and +623.04 with an average cumulative ε_{RMSE} being 65.85 and efficiency after Nash-Sutcliffe[6] of 0.88. Considering this, it is clear that the range of the prediction errors is quite staggering. Mostly affected in this regard is the peakflow forecast; the variations in the simulated discharges relative to the observed with respect to high flows are significant. This discrepancy is elucidated more clearly in the visual plot as shown in Fig. 4. From Fig. 4, it is apparent that information sharing among input variables is best at low flows and as the magnitude of flow increases, the residual also appreciates significantly.

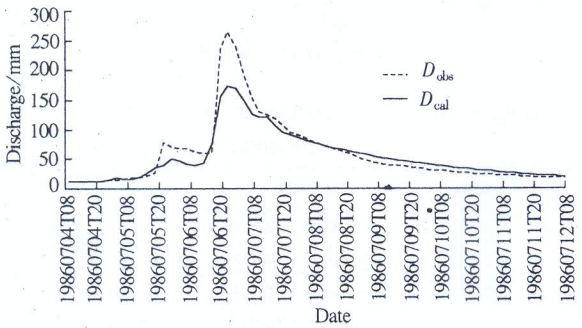

Fig. 3 Flood event hydrograph

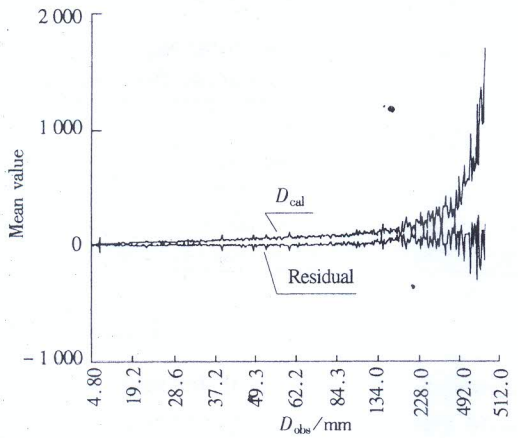

Fig. 4 Multiple Line Chart

Though the overall model performance efficiency is high, there exists a contrasting phenomenon here as shown in Tabs. 7 to 10. The coefficient of efficiency R^2 value for some flood events is high, denoting excellent prediction but this does not translate into better ε_{RMSE} values which measure the residual variance (For instance, flood events 3 and 16 in the calibration and verification stages for the Misai and Lushi catchments) (see Tabs. 7 to 10). The only objective explanation for this could be that the coefficient of efficiency of the R^2 statistic is oversensitive to extreme values because of the squared differences in its definition and correspondingly too, its insensitivity to additive and proportional differences between predictions and observations. The implication of this is that it leads to an increasing influence of large floods on the calibrated parameter values and invariably, as a result, tend to enhance the forecast accuracy of the larger floods.

In the second phase of the study, the ANN model was used. It is glaring from Tabs. 3 and 4 that using the 3-hourly and hourly flood data, the inter-variable correlation is almost insignificant but for intra-variables, a certain degree of correlation is discernible; at least for a one time step (i. e. 3 h). The only conclusion here is that the combination of these input variables as lagged plays definitive interrelated roles in the net output predictions of the neural network.

Overall, the performance of the error correction model (the ANN model) operated on top of the Xin'anjiang conceptual model is distinctly excellent. The overall accuracy of the complementary model in this regard was evaluated by calculating ε_{RMSE}, coefficient of efficiency R^2, and correlation coefficients as in previous analyses. The ε_{RMSE} statistic whose optimal value is 0, for the Xin'anjiang model operated on a stand-alone basis both in the calibration and verification modes (the Misai catchment) performed below the complementary (see Tab. 11) in both cases. But for different variants of the complementary model, the ε_{RMSE} and R^2 values are much better relatively. On the other hand, for the correlation statistic (optimal value is 1.0) which measures the linear correlation between the observed and the simulated flows, the complementary model reasonably performed better (see Tab. 5). The visual effect of this perfect fit can be seen in Figs. 5 and 6. In Fig. 5, the observed discharge D_{obs} is completely eclipsed by the adjusted discharge D_{corr}; this connotes effective correlation. Similarly, Fig. 6 shows a close reproduction of the prediction error from the conceptual model; Tab. 5 attests to this phe

nomenon. This scenario is also typically reproduced using the hourly flood data in the Lushi basin (see Tab. 12). As discussed in the preceding section for the Misai catchment, here too, the performance of the ANN complementary model operating on top of the Xin'anjiang model outweighs that of the latter on a stand-alone basis (see Tabs. 6 and 12).

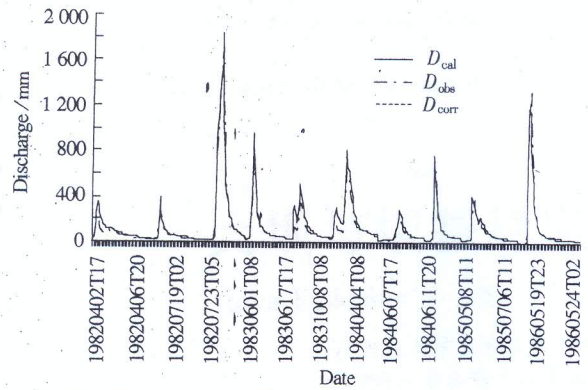

Fig. 5 D_{corr} along the Xin'anjiang model D_{obs} and D_{cal}

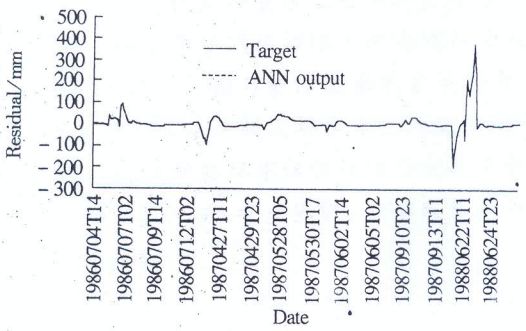

Fig. 6 Error prediction

Tab. 11 The performance of different models for the Misai catchment

Model variant	Data set	ε_{RMSE}	R^2
Xin'anjiang model	1st half (calibration)	50.42	0.86
	2nd half (verification)	32.71	0.85
ANN model Ⅰ + Xin'anjiang model	1st half (training)	0.029	0.99
	2nd half (verification)	0.044	0.93
ANN model Ⅱ + Xin'anjiang model	1st half (training)	26.030	0.72
	2nd half (verification)	26.020	0.73

Tab. 12 The performance of different models for the Lushi catchment

Model variant	Data set	ε_{RMSE}	R^2
Xin'anjiang model	1st half (calibration)	75.24	0.89
	2nd half (verification)	43.37	0.85
ANN model + Xin'anjiang model	1st half (training)	28.10	0.93
	2nd half (verification)	29.98	0.89

6 Conclusion

Results obtained from both the calibration and verification stages for the two cases, namely Misai and Lushi, indicate that the SCE algorithm is capable of finding a conceptually realistic and valid parameter set in the automatic calibration of the Xin'anjiang model. In all, given the inherent errors in calibration and validation data, model inadequacies by many simplifying assumptions and obtaining a set of global optimum parameters through any automatic calibration procedures are a remote possibility or rather a seeming mirage. This becomes manifest at least considering the SCE algorithm for instance. The SCE algorithm has some inexplicable explanations about the steps it follows; sometimes the objective function evaluations become useless because it has to undergo reflection, expansion, and contraction steps by a single set of points in one sub-complex evaluation. In so doing, the values obtained are discarded in the process. This procedure is somewhat ambiguous and deserves further explanation and simplification.

The final part of this study involves the use of the ANN model on top of the Xin'anjiang model to enhance its prediction. As is typical, the acceptance/rejection of an ANN model is based on its ability to generalize its predictions to new data sets not previously used in the training and thus unfamiliar with the model. In all, for the two catchments, the performance of the error prediction model outweighs that of the Xin'anjiang model (see Tabs. 5 and 6) operating alone on the basis of the aforementioned criteria. The results indicate that the proficiency of the artificial neural network is able to generalize quite well. Concisely, from the results it can be concluded that the application of the complementary models to forecast the residual errors of conceptual models improves the run-off or discharge forecasts considerably. Considering this, as far as the Xin'anjiang model is concerned under this application, the gain allowed by the introduction of the ANN model, through the addition of discharge updating is remarkable. This is obvious in view of the differences in the goodness-of-fit criteria between the Xin'anjiang model forecast and the error correction ANN model operating on top of it.

Acknowledgement The authors are pleased to acknowledge the support of A. P. Hapuarachchi in putting together the data used here for analysis and more importantly too, his incisive and instructive comments.

References

[1] Abebe A J, Price R K. Enhancing flood forecasts via complementary modeling [A]. In: *Flood Defence Conference*

References

[1] Du Chengbin, Ren Qingwen. Nonlinear finite element analysis of dam with perimentral joints [A]. In: *Proc of Computational Mechanics* [C]. Philippines, 2000, **1**: 346.

[2] Dawson E M, Roth W H, Drescger A. Slope stability analysis by strength reduction [J]. *Journal Geotechnical*, 1999, **49** (6): 835 - 840.

[3] Du C B, Qiu Y. Analysis of failure of Meihua arch dam [A]. In: *Proc of the 3rd International Conference on Dam Engineering* [C]. Singapore, 2002. 89 - 96.

[4] Zienkiewicz O C, Valliappan S, King I P. Elasto-plastic solution of engineering problems initial stress, finite element approach, international [J]. *Journal for Numerical Methods in Engineering*, 1969, **1**: 75 - 100.

[5] Owen D R J, Hinton E. *Finite elements in plasticity theory and practice* [M]. London: London University Press, 1980. 213 - 236.

大坝与坝基稳定性分析研究

Itoya Emioshor[1] 赵 引[1] Martins Y. Otache[2]

([1] 河海大学土木工程学院, 南京 210098)
([2] 河海大学水资源环境学院, 南京 210098)

摘要: 大坝与坝基的稳定一直是工程师密切关注的一个安全问题. 论文提出 2 种分析重力坝和坝基稳定的方法: 一种是基于刚体极限平衡原理的直接分析方法, 它将坝体和岩基作为不变形的刚体, 利用该方法可直接计算出可能滑动面的安全因数; 另一种是基于弹塑性理论的间接分析方法, 它采用非线性有限元方法分析大坝和坝基的应力和变形. 根据收敛和突变准则来确定稳定安全度.结果表明: 工程建筑物的破坏不仅仅是由于施加荷载的原因, 同时也与组成材料的性质有关.

关键词: 稳定性; 重力坝; 安全因数; 刚体极限平衡原理; 弹塑性理论; 非线性有限元方法

中图分类号: TV642